Modeling and optimization of reactant gas transport in a PEM fuel cell with a transverse pin fin insert in channel flow

S. O. Obayopo, T. Bello-Ochende* and J. P. Meyer

Department of Mechanical and Aeronautical Engineering, University of Pretoria, Pretoria, Private Bag X20, Hatfield, 0028, South Africa.

Abstract:

A proton exchange membrane (PEM) fuel cell has many distinctive features which makes it an attractive alternative clean energy source. Some of those features are low start-up, high power density, high efficiency and remote applications. In the present study, a numerical investigation was conducted to analyse the flow field and reactant gas distribution in a PEM fuel cell channel with transversely inserted pin fins in the channel flow aimed at improving reactant gas distribution. A fin configuration of small hydraulic diameter was employed to minimise the additional pressure drop. The influence of the pin fin parameters, the flow Reynolds number, the gas diffusion layer (GDL) porosity on the reactant gas transport and the pressure drop across the channel length were explored. The parameters examined were optimized using a mathematical optimization code integrated with a commercial computational fluid dynamics code. The results obtained indicate that a pin fin insert in the channel flow considerably improves fuel cell performance and that optimal pin fin geometries exist for minimized pressure drop along the fuel channel for the fuel cell model considered. The results obtained provide a novel approach for improving the design of fuel cells for optimal performance.

Keywords: PEM fuel cell; Reactant gas; Pin fin; Pressure drop; Flow resistance, Mathematical optimisation

* Corresponding author. Tel.: +27124203105; fax: +27 (0) 12 362 5124.
E-mail address: Tunde.Bello-Ochende@up.ac.za

1. Introduction

The flow distribution in a fuel cell bipolar plate is one of the most important enhancing factors of proton exchange membrane (PEM) fuel cell systems. One of the critical issues in PEM fuel cell design is the efficient design of the flow channels to ensure uniform distribution of the reactant gases in the fuel cell stack. The flow field geometry and pattern have great influence on the reactant gas transport, water management and the efficient utilization of the fuel. The flow field design of fuel cells is one of the critical technical challenges for PEM fuel cell designs and operation and impacts on the performance and the life - span of the system [1,2].

Nomenclature

A^c	Fin cross-sectional area [m^2]
A_{ch}	Channel cross-sectional flow area [m^2]
C	Constant
C_F	Quadratic drag factor
c_r	Condensation rate constant
D_f	Diameter of pin fin [m]
D_{ch}	Channel diameter [m]
D	Gas mass diffusivity [$m^2\ s^{-1}$]
f	Friction factor
h	Height
H	Computational domain height[m]
k	Permeability
L	Channel axial length [m]
M	Molar mass [g/mol]
$\dot{m}$	Channel mass flow rate [kg/s]
P	Pressure [Pa]
P_o	Poiseuille constant
P_{pump}	Pumping power [W]
Q	Volume flow rate [m^3/s]
r_w	Water condensation rate [s^{-1}]

R	Universal gas constant [8.314 J mol/K]
Re	Reynolds number
R_f	Dimensionless flow resistance
s_w	Water saturation
s	Pin spacing [m]
t	Time [s]
T	Temperature [K]
Uo	Average velocity at inlet [m/s]
u,v	Velocities in the x- and y- directions [m/s]
x,y	Cartesian coordinates [m]
V	Volume [m^3]
V_d	Volume ratio in diffusion layer
V_s	Surface ratio in diffusion layer
w	Mean velocity [m/s]
W	Molar mass fraction of oxygen

Greek Symbols

Δ	Difference
ε	Porosity
μ	Dynamic viscosity [kg/m.s]
υ	Viscosity of flow [kg m^{-1} s^{-1}]
ρ	Density [kg/m^3]
λ	Tip clearance ratio
ν	Kinematic viscosity [m^2 s^{-1}]
ζ	Pitch
τ	Tortuosity
φ	Solid fraction

Subscripts

ch	Channel
d	Porous diffusion layer
eff	Effective

h	Hydraulic
l	Liquid water
max	Maximum
min	Minimum
opt	Optimum
sat	Saturation
w	Liquid water phase

Several studies have been carried out in recent years to improve fuel cell performance through flow-field design such as parallel, serpentine, interdigitated and many other novel combinations of these conventional types [3-10]. The serpentine channel type is the most widely used among the studied flow channels due to its outstanding performance when compared with others under the same operating and design conditions [11].

However, a serpentine flow field has its associated problems and is not an ideal flow field configuration. Some of the associated problems are: (i) high reactant pressure loss resulting in significant parasitic power requirement to pressurize air especially at the cathode section [12], (ii) loss of reactant gas concentration along the channel from inlet towards the outlet and membrane dehydration near the channel inlet region, and (iii) resultant liquid water flooding near the exit region of the channel as a result of excessive liquid water carried downstream of the channel by the reactant gas stream and collected along the flow channel [13].

These characteristics of serpentine flow channels proved their effectiveness in small cells ($\leq 560 \times 250 \times 330$ mm and power rating ≤ 1000 W) where the pressure drop is in the order of 0.5-1 bar. However, serpentine flow channels perform poor for larger cells ($> 560 \times 250 \times 330$ mm and power rating ≥ 1500 W) where the pressure drop is in the order of a few bars [14]. Hence, parallel flow channels have several applications especially for larger cell applications but the problems of cathode gas flow distribution and cell water management need to be solved.

In these channels, apart from issues related to maldistribution of reactant gases, water coalescence forms droplets of varying number and sizes in the channels. This subsequently forces the reactant gas to flow preferentially through the path of least obstruction [15]. Performance improvements for this type of channel and others

have been documented in the literature, but there is little information in the open literature regarding the design procedure and cross-sectional dimensions including pressure drops for flow in the channels [12]. Performance improvement of PEM fuel cells can be achieved in many ways and researchers have developed varieties of flow field layout for this purpose.

An interdigitated flow field design was first proposed by Nguyen [16] with addition of baffles at the end of the channels. The design forces the reactants through the gas diffusion layer (GDL) and the generated shear forces help blow the trapped water in the inner layer of the electrodes resulting in better performance of the fuel cell.

Kumar and Reddy [17] presented a three-dimensional steady-state numerical mass-transfer single cell model for a PEM fuel cell using metal foam in the flow-field of the bipolar/end plates rather than using conventional rectangular channels. Their result showed significant effect of the metal foam on permeability of the reactant species, thereby improving the performance of the fuel cell. They proposed the use of metal foam instead of conventional rectangular channels especially in thinner channels where there are manufacturing constraints.

Liu *et al.* [18] investigated the effect of baffle-blocked channels on the reactant transport and cell performance using a conventional parallel flow field. Their results showed improved cell performance due to increasing reactant spread over the GDL, which enhances chemical reactions.

Soong *et al.* [19] developed a novel flow channel configuration by inserting baffles in the channel of conventional flow fields to form a partially blocked fuel channel. They discovered that enhanced fuel cell performance could be achieved by reducing the gap size and/or increasing the baffle number along the channel though with penalty of higher pressure loss.

Liu *et al.* [20] studied the reactant gas transport and cell performance of a PEM fuel cell with a tapered flow channel design. The results obtained from the study revealed that fuel cell performance can be enhanced with the fuel channel tapered and enhancement is more prominent at lower cell voltage. The reactant gas in the tapered channel is accelerated and forced into the gas diffusion layer, thereby enhancing the electrochemical reaction that improves the cell performance.

Xu and Zhao [21] presented a new flow field design termed convection-enhanced serpentine flow field (CESFF) for polymer electrolyte-based fuel cells.

They observed that the CESFF design induces larger pressure differences between adjacent flow channels over the electrode surface when compared with the conventional flow field. This characteristic of the design increases the mass transport rates of reactants and products to and from the catalyst layer and reduces liquid water entrapped in the porous electrode and subsequently, enhances the fuel cell performance.

Wang *et al.* [22] similarly studied the use of baffles in a serpentine flow field to improve cell performance. The results showed that the novel baffle serpentine flow field, even though induces larger pressure differences between adjacent flow channels over the entire electrode surface than does the conventional serpentine design; helps gas diffusion which leads to enhanced current density and improved cell performance.

These investigations have shown that fuel cell performance can be enhanced through addition of bluff bodies (baffles) in the flow channels to increase the convection of reactants through the GDL. This enhanced performance and operating stability in the fuel cell are achieved through improved reactant mass transport. Meanwhile, a proper understanding of the phenomenon of mass transfer through the GDL, under the influence of disturbances along the flow channels and associated pressure drop, will facilitate a proper design of PEM fuel cells.

From the literature survey above, it is clear that issues of high penalty in terms of pressure loss due to high flow resistance do occur in most of the baffle-enhanced PEM flow field designs, which need to be alleviated. In addition, to the best knowledge of the authors, the application of pin fins for performance enhancement in PEM fuel cell has not been examined before especially determining the optimal geometry of the employed pin fins in PEM flow channels. Therefore, the purpose of this study is to investigate the effect of a pin fin insert in the flow field of a fuel cell with the aim of improving performance as well as pressure drop along the fuel cell flow channel. The cell overpotential at the anode side of the PEM fuel cell is negligible in comparison with the cathode-side overpotential [23], hence the choice of considering oxygen mass transport at the cathode side of the fuel cell system. Extended surfaces (fins) are frequently used in heat exchanging devices for the purpose of increasing the heat transfer between the primary surface and the surrounding fluid. Extended surfaces of various shapes have been employed for this purpose in heat and mass transfer studies, ranging from relatively simple shapes, such as rectangular, square, cylindrical, annular, tapered or pin fins, to a combination of

different geometries. Literature shows that pin fins are some of the most widely employed extended surfaces looking at its hydrodynamics along flow channels [24-28]. A pin fin is a cylinder or other shaped element attached perpendicularly to a wall, with the transfer fluid passing in cross-flow over the element. Pin fins having a height to diameter ratio between 0.5 and 4 are accepted as short fins, whereas long fins have a pin height to diameter ratio exceeding 4 [25]. The effective selection of the pin fin geometric parameters will result in the improvement of the reactant gas distribution in the flow channel due to the mixing of the main flow and/or the flow in the near-wall region and subsequently, will permit effective reactant spread on the GDL.

In the present work, it is intended to investigate the effect of pin fins transversely arranged along the flow channel on the reactant gas distribution and pressure drop characteristics of the fuel cell reactant gas channel. Pin fins of small hydraulic diameter, which can reduce the additional pressure drop, are employed and the effect on PEM performance is investigated. In addition, a mathematical optimization tool is used to select the best pin fin geometric configuration that improves the fuel cell performance at a reduced pumping power requirement penalty in the PEM fuel cell flow channel. This study presents a novel approach at enhancing the oxygen mass transfer through the PEM fuel cell GDL at reduced pressure drop.

2. Model description

In this study, a two-dimensional half-cell model of a PEM fuel cell system for the cathode-side fuel gas channel and the GDL is considered. Fig. 1 shows a schematic diagram of the two-dimensional half-cell model with two pin fins along the transverse section of the flow channel. The fluid considered here is air at an inlet pressure P_0 and velocity U_0. The fin disturbance employed in this study protrudes from a rectangular base towards the gas diffusion layer having a height to diameter ratio between 0.5 and 4. The parameters h_1, h_2 and h_3 (Fig. 1) depict the flow channel height, tip clearance size and GDL thickness, respectively. The tip clearance size is characterized by defining a dimensionless parameter named clearance ratio, $\lambda \equiv h_2/h_1$, for the study. The values of $\lambda = 0$ and 1 indicate fully blocked and block-free conditions, respectively, and the values in between are a measure of various levels of blockage [19]. Also defined is another dimensionless parameter: the ratio of the distance

between pin distances in the transverse direction to fin thickness (pitch), $\zeta = s/d$. The effects of the tip clearance size, the pitch, the fuel flow Reynolds number (Re) and the porosity (ε) of the GDL on the reactant gas transport and the pressure drop across the channel are critically explored. The porosity, ε , of the porous medium is defined as the fraction of the total volume of the medium that is occupied by void space. In this study, parameters were varied in the following range: $0.2 \le \lambda \le 0.6$, $5.0 \le \zeta \le 10$, $50 \le Re \le 350$ and $0.2 \le \varepsilon \le 0.6$. Other parameters used for the modeled PEM fuel cell are shown in Table 1. The idea in this paper is aimed at improving the reactant species distribution over the catalyst layer in the fuel cells to increase the fuel cell performance at reduced pumping power requirement.

2.1 Governing equations

The present study provides a two-dimensional solution for the half-cell model of a PEM fuel cell. The following assumptions are used in this study: (1) the reactant gas (air) is an ideal gas, and the flow is incompressible, steady and laminar, (2) the gas diffusion layer is from an isotropic porous material and uniform, (3) the catalyst layer is treated as an ultra-thin layer (regarded as a boundary condition), hence the reactant gas is totally consumed in the reaction, (4) the reaction is assumed to be fast ensuring that the transport time scale is dominant when compared with the reaction time scale. This assumption allows treating the chemical reaction simply as a boundary condition at the catalyst layer, (5) the fuel cell operates at a constant temperature. Based on these assumptions, the following governing equations for the gas channel and the gas diffusion layer can be written as [29]:

In the gas channel section, the governing equations are:

$$\frac{\partial u}{\partial x} + \frac{\partial v}{\partial y} = 0, \tag{1}$$

$$u\frac{\partial u}{\partial x}+v\frac{\partial u}{\partial y}=-\frac{1}{\rho}\frac{\partial P}{\partial x}+\nu\left(\frac{\partial^2 u}{\partial x^2}+\frac{\partial^2 u}{\partial y^2}\right), \tag{2}$$

$$u\frac{\partial v}{\partial x}+v\frac{\partial v}{\partial y}=-\frac{1}{\rho}\frac{\partial P}{\partial y}+\nu\left(\frac{\partial^2 v}{\partial x^2}+\frac{\partial^2 v}{\partial y^2}\right), \tag{3}$$

$$u\frac{\partial W_i}{\partial x}+v\frac{\partial W_i}{\partial y}=D_i\left(\frac{\partial^2 W_i}{\partial x^2}+\frac{\partial^2 W_i}{\partial y^2}\right), \tag{4}$$

where D_i and W_i depict the diffusivity and mass fraction of the species, respectively.

In the GDL section, the governing equations are:

$$\frac{\partial u}{\partial x}+\frac{\partial v}{\partial y}=0, \tag{5}$$

$$\varepsilon\left(u\frac{\partial u}{\partial x}+v\frac{\partial u}{\partial y}\right)=-\frac{\varepsilon}{\rho}\frac{\partial P}{\partial x}+\upsilon\varepsilon\left(\frac{\partial^2 u}{\partial x^2}+\frac{\partial^2 u}{\partial y^2}\right)-\frac{\upsilon\varepsilon^2}{k}u-\frac{\varepsilon^3 C_F\rho u}{\sqrt{k}}\sqrt{u^2+v^2} \tag{6}$$

$$\varepsilon\left(u\frac{\partial v}{\partial x}+v\frac{\partial v}{\partial y}\right)=-\frac{\varepsilon}{\rho}\frac{\partial P}{\partial y}+\upsilon\varepsilon\left(\frac{\partial^2 v}{\partial x^2}+\frac{\partial^2 v}{\partial y^2}\right)-\frac{\upsilon\varepsilon^2}{k}v-\frac{\varepsilon^3 C_F\rho v}{\sqrt{k}}\sqrt{u^2+v^2} \tag{7}$$

$$\varepsilon\left(u\frac{\partial W_i}{\partial x}+v\frac{\partial W_i}{\partial y}\right)=D_{i,eff}\left(\frac{\partial^2 W_i}{\partial x^2}+\frac{\partial^2 W_i}{\partial y^2}\right) \tag{8}$$

C_F in Eqs. (6) and (7) depicts the quadratic drag factor. The Blake-Kozeny correlation [19,30] is used for the relationship between the porosity ε and permeability k of the GDL:

$$k=\left(\frac{D_d^2}{150}\right)\left[\frac{\varepsilon^3}{(1-\varepsilon)^2}\right] \tag{9}$$

where

$$D_d\equiv\frac{6V_d'}{S_d'} \tag{10}$$

The last two terms in Eqs. (6) and (7) are drag force terms added due to the presence of the porous wall, which might increase the pressure drop. The porous diffusion layer quantity is represented by the subscript *d* and $V_d^{'}/V_s^{'}$ is a geometrical parameter which depicts the volume-to-surface ratio of the gas diffusion layer [19]. In fuel cells, the fluid flow diffuses through the GDL for the reaction to take place on the MEA. The effective diffusivity $(D_{i,eff})$ for gas-phase flow in porous media can be written as:

$$D_{i,eff} = D\frac{\varepsilon}{\tau} \tag{11}$$

The porosity ε is the void volume fraction in the porous media. The tortuosity, τ, is a measure of the average path length of the species flow through the porous media compared to the linear path length in the direction of the species transport. The quantity (tortuosity) is usually estimated through experiment. Therefore, it is conventionally correlated in fuel cell studies using the Bruggeman correlation. This correlation assumes τ is proportional to $\varepsilon^{-0.5}$ resulting in the simpler expression [31]:

$$D_{i,eff} = D\varepsilon^{1.5} \tag{12}$$

The porosity correlation is used to account for geometric constraints of the porous media.

The Reynolds number was defined as [32]:

$$\mathrm{Re} = \dot{m}D_{ch}/(\mu A_{ch}) \tag{13}$$

For hydraulic performance in the channel, an apparent friction factor f was evaluated using the following equation [32]:

$$f = (\Delta P / L)D_{ch}/(\rho w^2/2) \tag{14}$$

where

$$w = \dot{m}/(\rho A_{ch}) \tag{15}$$

The channel flow resistance, $(\Delta P/\dot{m})$, is defined as [33]:

$$R_f = 2Po\nu L/D_{ch}^2 A_{ch} \tag{16}$$

where Po is the Poiseuille constant.

The pumping power is evaluated using the relation:

$$P_{pump} = \int_0^L \left[\frac{dp(x)}{dx} Q(x) \right] dx \tag{17}$$

The water formation and transport of liquid water are modeled using a saturation model based on [34,35]. In this approach, the liquid water formation and transport are governed by the conservation equation for the volume fraction of liquid water s_w or the water saturation [36]:

$$\frac{\partial(\varepsilon \rho_l s_w)}{\partial t} + \nabla \cdot (\rho_l \vec{V}_l s) = r_w \tag{18}$$

where the subscript l represents liquid water, and r_w is the condensation rate modeled as:

$$r_w = c_r \max\left(\left[(1 - s_w) \frac{P_{wv} - P_{sat}}{RT} M_{w,H_2 0} \right], [-s_w \rho_l] \right) \tag{19}$$

where r_w is added to the water vapour equation. The condensation rate is constant at $c_r = 100 s^{-1}$.

The clogging of the porous media and the flooding of the reaction surface are modelled by multiplying the porosity and the active surface area by $(1 - s_w)$, respectively.

2.2 Numerical procedure

The model equations were solved using a finite-volume computational fluid dynamics code Fluent [36] with Gambit® (2.4.6) as a pre-processor. The CFD code has an add-on package for fuel cells, which has the requirements for the source terms for species transport equations, heat sources and liquid water formations. The domain was discretized using a second-order discretization scheme. The pressure-velocity coupling was performed with the SIMPLE algorithm [37] for convection-diffusion analysis. Numerical convergence was obtained at each test condition when the ratio of the residual source (mass, momentum and species) to the maximum flux across a control surface was less than 10^{-6}.

Uniform isothermal free stream and fully developed fluid (air) with constant properties were assumed at the inlet and flows were fully developed at the outlet of the channel. At the interface between the gas channel and the GDL layer interface, the same velocity, the same concentration and the same gradients were imposed. No-slip, no-penetration boundary conditions were enforced on the pin fins and wall surfaces.

The domain was divided into hexahedral volume elements. A grid independence test was carried out to ensure that solutions were independent of the dimensions of the chosen grid with consideration for both accuracy and economics. For this purpose, four grid systems at 37 × 27, 82 × 27, 120 × 60 and 150 × 80 were tested. For the case of *Re* = 350, $\lambda = 0.6$, $\zeta = 7.0$ and $\varepsilon = 0.5$, the maximum relative deviation for the skin friction between the 120 × 60 grid and the 150 × 80 grid was less than < 3%. It was considered that the system of 120 × 60 was sufficient enough for the study as a trade-off between accuracy and cost of time. A typical grid network for the computational domain is shown in Fig. 2. The model and solution were implemented using an Intel® Core(TM) 2Duo 3.00 GHz PC with 3.24 GB of DDRam.

3. Mathematical optimisation algorithm

The Dynamic-Q optimization algorithm [38] was used in this study. The algorithm is a robust multidimensional gradient based optimization algorithm which does not require an explicit line search and it is ideally robust for cases where the function evaluations are computationally expensive. The algorithm applies the dynamic

trajectory LFOPC (Leapfrog Optimisation Program for Constrained Problems) which is adapted to handle constrained problems through approximate penalty function formulation [38]. This dynamic approach is applied to successive quadratic approximations of the actual optimization problem. The successive sub-problems are formed at successive design points by constructing spherically quadratic approximations which are used to approximate the objective functions or constraints (or both) if they are not analytically given or very expensive to compute numerically [39-41]. The use of spherically quadratic approximation in the Dynamic-Q algorithm offers a competitive advantage when compared with other algorithm in term of the computational and storage requirements [39]. The storage savings becomes highly significant when the number of variables becomes large. Therefore, this particular strength of the Dynamic-Q method makes it well suited for optimisation of engineering problems with large number of variables and it has been used to successfully solve a large variety of engineering problems [41,42-47].

4. Optimisation problem formulation

The optimization problem was tailored towards finding the best pin fin geometric parameters, which give the best reactant species diffusion to the GDL layer of the fuel cell for a fixed Reynolds number, GDL thickness and GDL porosity at a reduced channel flow resistance contributing to the increase in pressure drop along the channel. The apparent pressure drops increase the pumping power requirement for operating a fuel cell system. The design variables which greatly affect the hydrodynamic performance of pin fins are the geometric parameters $s, d, h_2,$ and h_1 as depicted in the half-cell model shown in Fig. 1.

4.1 Optimisation constraints

The optimization problem was carried out subject to the following constraints:

4.1.1 *Total pin fin area constraint*: In pin fin application, the weight and material cost of the pin fins are limiting factors. Hence, the total area of the pin fins is fixed to a constant value:

$$\therefore \sum A^c{}_j = \text{Constant}$$

$$\sum \pi D_j H_j = C$$

$$\sum D_j H_j = \frac{C}{\pi} \quad (26)$$

for $j = 1, 2$

where A^c is the pin fin area.

4.1.2 The tip clearance size: The tip clearance size λ is the ratio of the gap size between the pin fin tip and the GDL to the channel height. This was varied between 0.2 and 0.6.

$$0.2 \le \left[\lambda = \frac{h_2}{h_1} \right] \le 0.6 \quad (27)$$

4.1.3 The pitch: The pitch is the ratio of the distance between successive pin fins to the pin fin diameter. This is allowed to vary between 5 and 10.

$$5 \le \left[\zeta = s/d \right] \le 10 \quad (28)$$

4.1.4 Manufacturing constraint: The solid area fraction φ, which is defined as the ratio of the pin fin material to the total area of the fuel cell channel is allowed to vary between 0.5 and 4. This is based on manufacturing and size constraints [48,49].

$$0.5 \le \left[\varphi = \frac{h_1 - h_2}{d} \right] \le 4 \quad (29)$$

Also, the interfin spacing is limited to 50 microns based on pin fin fabrication techniques [50,51].

$$s \ge 50 \mu m \quad (30)$$

4.2 Optimization procedure

The optimization problem defined in Section 4.1 was solved by coupling the Dynamic-Q optimization algorithm with computational fluid dynamics code FLUENT [36] and grid generation (GAMBIT [52]) code in a MATLAB [53] environment. Fig. 3 depicts a flow diagram of how the automation is carried out until convergence (either by step size or function value criteria) is attained. To ensure that the converged solution obtained is indeed the global minimum, a multi-starting guess approach was employed.

5. Results and discussion

5.1 Results of flow field

The pin fins employed in this work are expected to induce high levels of mixing of main flow and/or the flow in the near-wall region and subsequently to improve the convection of reactant gas through the GDL. The power output in fuel cell system is the consequence of the electrochemical reaction; subsequently, the consumption of oxygen through diffusion into the catalyst membrane region is an index of the cell performance [22]. Higher oxygen mass flow rates through the GDL to the catalyst layer result in better fuel cell performance since this reaction gas is more available to participate in the electrochemical reaction per unit time. A qualitative description of the flow velocity pattern around the pin fin and within the GDL is presented in Figs. 4-6 to give the impression of the hydrodynamic phenomenon in the computational domain.

Fig. 4 shows the Reynolds number influence on the flow pattern for the case of s/d = 5, and $\lambda = 0.2$ at a fixed GDL porosity of 0.5. The Reynolds number has a significant effect on the flow field and the diffusion of the reactant gas through the GDL medium. The rate of diffusion increases as the Reynolds number increases thereby improving the reaction rate in the fuel cell system. The wake shedding generated by the front pin fin interacts with the pin fin immediately behind it along the channel, which affects the flow field characteristics. At a low Reynolds number of 50 (Fig. 4a), there is flow attachment between the front pin and the back pin tips. This

flow attachment also occurs at a Reynolds number of 150 (Fig. 4b), but for a Reynolds number of 250, a flow separation occurs at the tip between the front pin and the back pin. This phenomenon at the increased Reynolds number increases the wake generation and the diffusion pattern into the GDL layer of the cell. The angle of separation of flows depends on the Reynolds number and level of clearance ratio. As the clearance ratio increases, the location of the boundary layer separation moves forward. This movement is practically due to the change in the velocity distribution inside the boundary layer formed on the pin fins.

The flow pattern for a higher tip clearance ($\lambda = 0.6$) is shown in Fig. 5, where the effect of the Reynolds number (at fixed GDL porosity of 0.5) can also be clearly observed. The flow pattern in Fig. 5 depicts the significant influence of the increase in the tip clearance between the pin fin and the GDL layer on the rate of reactant diffusion through the GDL into the catalyst reaction site. The reactant gases are forced down the GDL hence improving the rate of electrochemical reaction to improve the performance. In Fig. 6, the contours of the tangential velocity profiles for the same case described in Fig. 5 are shown. High pressure points are shown at the tips of the front pin. The rate of reactant gas diffusion into the GDL improves from Contours (a) to (c).

5.2 *Results of pin fin geometry*

Fig. 7 presents the friction factor *f* as a function of the channels Reynolds number and the pitch (ratio of distance between the pin fin and the pin fin diameter). The friction factor decreased with increasing Reynolds number. The data obtained in Fig. 7 further shows that as the pitch increases, the friction factor decreases. This implies lower diffusion of reactant gas, which reduces performance of the fuel cell. Hence, lower pitch value, which generates more flow disturbance between the pin fin tip and GDL surface will be more appropriate as this improves the fuel transport rate and subsequently, the reaction rate at the catalyst layer is improved, but this should also be optimised for minimum power requirement.

Fig. 8 shows the variation of the friction factor as a function of the channel Reynolds number and the clearance ratio (λ) between the pin fin and the GDL surface. Decreasing λ means that the height of the fin towards the GDL increases. Similarly, decreasing the height of the fin reduces the pressure drop in the gas channel

flow and subsequently reduces convectional flow through the fuel cell GDL thereby reducing the cell performance. Increasing the height of the pin fin increases the fluid flow into the reaction site of the fuel cell. This is due to the tangential flow velocity created by the pin fin and flow mixing effects, however, with a penalty of increasing pumping power requirement due to increased pressure drop along the fuel channel. This is also supported by the flow description experienced at higher λ in Fig. 5. An optimised clearance ratio will reduce the associated pressure drop due to the increase in pin length towards the GDL and pumping cost will be reduced.

Fig. 9 depicts the friction factor as a function of channel Reynolds number and the GDL porosity. The results show a decrease in the friction factor with an increase in the GDL porosity of the fuel cell. The increased GDL porosity improves the convection flow through the GDL and subsequently improves the fuel cell performance. The flow resistance in the channel at the larger GDL porosity (e.g. 0.7) was much less than with the smaller porosity (e.g. 0.3). The pressure drop along the flow channel enhanced with pin fins can be considerably reduced with an appropriate higher GDL porosity.

Fig. 10 shows the peak channel flow resistance as a function of the clearance ratio and the GDL porosity. There is an optimum clearance ratio at $\lambda \approx 0.39$ in which the peak flow resistance in the fuel gas channel is minimised. Also, Fig. 11 shows the peak channel flow resistance as a function of the pitch and the GDL porosity. There is also an optimal pitch at $s/d \approx 7.8$, which minimises the fuel channel friction. These results support the fact that an optimal arrangement of the pin fin parameters could effectively minimise the fuel channel friction and reduce the pressure drop along the fuel channel with a corresponding increase in reaction rate on the catalyst layer, thereby improving the fuel cell performance. Figs. 10 and 11 also show that the GDL porosity has a significant effect on the peak flow resistance along the fuel gas channel. An increase in the GDL porosity reduces the peak flow resistance in the fuel channel. This observation is in agreement with previous work of Soong *et al.* [19].

5.3 Optimisation results

In this section, the optimisation algorithm was applied to obtain the best geometric configuration of the pin fin that will offer optimal flow resistance along the fuel cell channel, ensuring the system performance at an optimum. From the results in Section

5.2, it is clear that the pin fin geometric parameters (clearance ratio and pitch) optimally exist, which minimises the channel flow resistance. This optimal geometric parameters and the porosity of the GDL have significant influence on the fuel cell performance through reactant gas distribution and reaction rate on the catalyst layer. Reducing the inherent flow resistance along the flow channel will reduce the additional pressure drop, therefore reducing the pumping power requirement. A series of numerical optimisations and calculations were conducted within the design constraint ranges given in Section 4.1 and the results are presented in the succeeding section to highlight the optimal behaviour of the fuel cell system.

Fig. 12 shows the effect of the minimised flow resistance as a function of the Reynolds number for a fixed clearance ratio of 0.3 and a GDL porosity of 0.5. Minimised flow resistance decreases with an increase in the Reynolds number. Fig. 13 shows that the optimal fin clearance ratio decreases as the Reynolds number increases. This result affirms the fact that there exists a unique optimal fin clearance ratio for the fuel gas Reynolds numbers. Similarly, Fig. 14 shows the optimal pitch as a function of the fuel gas Reynolds number at a fixed clearance ratio of 0.3 and a GDL porosity of 0.5. The result also shows the existence of a unique optimal pitch for the fuel gas Reynolds numbers.

The effect of channel flow resistance on the optimised channel clearance ratio at a porosity of 0.5, pitch of 5 and Reynolds number of 250 was investigated in Fig. 15. The result shows that channel flow resistance has a significant effect on the optimised clearance ratio. As the flow resistance increases, the optimal clearance ratio decreases. Also in Fig. 16, the effect of channel flow resistance on the optimised fin pitch was investigated at clearance ratio of 0.3, GDL porosity of 0.5 and Reynolds number of 250. The result shows that the optimised pitch also decreases with an increase in channel flow resistance. Generally, in this model, the flow resistance decreases when the Reynolds number increases. The optimal clearance ratio and pitch also decrease with increasing channel flow resistance, but an optimal level of these factors (clearance ratio and pitch) exists which minimises the flow resistance of reactant gases in the fuel cell gas channel.

5.4 Performance evaluation

Generally, in heat transfer studies using pin fins for enhancement, performance analysis is done using performance evaluation criteria [25,54]. Therefore, it is necessary to perform a similar analysis for this study and state the performance in terms of pressure drop for a fuel cell channel equipped with pin fins and one without pin fins. Fig. 17 shows the pressure drop characteristic for a fuel cell channel with and without pin fin. The figure shows that higher pressure drops occur in the fuel channel with pin fins than in the fuel channel without pin fins, as can be expected. However, the difference obtained along the flow channel for all the fin geometry cases considered in this study was less than 6%. Thus a critical assessment of the result of this study shows that in terms of both high performance enhancement and reasonable pressure drop in a fuel cell system, the pin-fin-enhanced fuel channel is a promising approach for the optimal design of a fuel cell system. Fig. 18 shows the pumping power as a function of the clearance ratio at a Reynolds number of 250 for a pitch of 5 and GDL porosity of 0.6. The pumping power is the product of the volumetric flow rate and pressure drop. The result shows that there is a minimum pumping power for the friction factor of the fuel channel at a fixed Reynolds number and specified pitch and GDL porosity of the fuel cell system. In general, the clearance ratio λ, which has a significant effect on the fuel gas flow, can be optimized to improve the fuel cell performance at a reduced pumping power requirement.

Conclusions

The enhancement of the reactant gas transport phenomenon in the gas flow channel of a half-cell model of a PEM fuel cell with pin fin insert was numerically investigated. The effect of the flow and geometrical parameters of the pin fin on the flow distribution in the GDL and friction characteristics in the channel were critically studied. Pumping power requirement at varying pin fin clearance ratios to evaluate the performance was also explored. The conclusions are summarized as:

- The flow Reynolds number had a significant effect on the flow field and the diffusion of the reactant gas through the GDL medium increased as the Reynolds number increased.
- The friction factor increased with increasing clearance ratio of the pin fin in the channel.

- The optimal clearance ratio and pitch for the considered fuel cell channel decreased with an increase in the fuel channel friction.
- The friction factor decreased with an increase in the GDL porosity. Hence, the channel friction and pressure drop can be significantly reduced with increasing GDL porosity.
- An optimal pin fin clearance ratio exists which offered minimum pumping power requirement.
- An enhanced fuel cell performance was achieved using pin fins in a fuel cell gas channel, which ensured high performance and low fuel channel pressure drop of the fuel cell system.

Acknowledgements

This work was supported by the University of Pretoria, NRF, TESP, EEDSM Hub, CSIR, and the Solar Hub of the University of Pretoria and Stellenbosch University.

References

[1] Peng L, Lai X, Liu D, Hu P, Ni J. Flow channel shape optimum design for hydroformed metal bipolar plate in PEM fuel cell. J Power Sources 2008;178: 223-30.

[2] Gamburzev S, Boyer C, Appleby AJ. Proceedings of the fuel cell seminar, 1998:556-9.

[3] Kasim A, Liu HT, Forges P. Modeling of performance of PEM fuel cell with conventional and interdigitated flow fields. J Appl Electrochem 1999;29:1409-16.

[4] Barreras F, Lozano A, Valino L, Marin C, Pascau A. Flow distribution in a bipolar plate of a proton exchange membrane fuel cell: experiments and numerical simulation studies. J Power Sources 2005;144:54-66.

[5] Kazim A, Forges P, Liu HT. Effects of cathode operating conditions on performance of a PEM fuel cell with interdigitated flow fields. Int J Energy Res 2003;27:401-14.

[6] Obayopo SO, Bello-Ochende T, Meyer JP. Three-dimensional optimisation of a fuel gas channel of a PEM fuel cell for maximum current density. Int J Energy Res 2011;DOI:10.1002/er.1935.

[7] Maharudrayya S, Jayanti S, Deshpande AP. Pressure drop and flow distribution in multiple parallel-channel configurations used in proton-exchange membrane fuel cell stacks. J Power Sources 2006;157:358-67.
[8] Ferng YM, Su A, Lu SM. Experiment and simulation investigations for effects of flow channel patterns on the PEMFC performance. Int J Energy Res 2008;32:12-23.
[9] Wang XD, Duan YY, Yan WM, Peng XF. Local transport phenomena and cell performance of PEM fuel cells with various serpentine flow field designs. J Power Sources 2007;172:265-77.
[10] Hontanon E, Escudero MJ, Bautista C, Garcia-Ybarra PL, Daza L. Optimization of flow-field in polymer electrolyte membrane fuel cells using computational fluid dynamics techniques. J Power Sources 2000;86:363-8.
[11] Watkins DS, Dircks KW, Epp DG. Novel fuel cell fluid flow field plate. US Patent No. 4988583, 1991.
[12] Li X, Sabir, I, Park J. A flow channel design procedure for PEM fuel cells with effective water removal. J Power Sources 2007;163:933-42.
[13] Wang CY, Fundamental Models for Fuel Cell Engineering. Chem Rev 2004; 104(10):4727-66.
[14] Maharudrayya S, Jayanti S, Deshpande AP. Flow distribution and pressure drop in parallel-channel configurations of planar fuel cells. J Power Sources 2005;144:94-106.
[15] Li X, Sabir I. Review of bipolar plates in PEM fuel cells: Flow field designs. Int J Hydrogen Energ 2005;30:359-71.
[16] Nguyen TV. A gas distributor design for proton-exchange-membrane fuel cells. J Electrochem Soc 1996;143:L103-L105.
[17] Kumar A, Reddy RG. Modeling of polymer electrolyte membrane fuel cell with metal foam in the flow-field of the bipolar/end plates. J Power Sources 2003;114:54-62.
[18] Liu HC, Yan WM, Soong CY, Chen F. Effects of baffle-blocked flow channel on reactant transport and cell performance of a proton exchange membrane fuel cell. J Power Sources 2005;142:125-33.
[19] Soong CY, Yan WM, Tseng CY, Liu HC, Chen F, Chu HS. Analysis of reactant gas transport in a PEM fuel cell with partially blocked fuel flow channels. J Power Sources 2005;143:36-47.
[20] Liu HC, Yan WM, Soong CY, Chen F, Chu HS. Reactant gas transport and cell

performance of proton exchange membrane fuel cells with tapered flow field design. J Power Sources 2006;158:78-87.
[21] Xu C, Zhao TS. A new flow field design for polymer electrolyte-based fuel cells. Electrochem Comm 2007; 9:497-503.
[22] Wang XD, Duan YY, Yan WM. Novel serpentine-baffle flow field design for proton exchange membrane fuel cells. J Power Sources 2007;173:210-21.
[23] Jeng KT, Lee SF, Tsai GF, Wang CH. Oxygen mass transfer in PEM fuel cell gas diffusion layers. J Power Sources 2004;138:41-50.
[24] Bello-Ochende T, Meyer JP, Bejan A. Constructal multi-scale pin fins. Int J Heat Mass Transfer 2010; 53:2773-79.
[25] Sara ON. Performance analysis of rectangular ducts with staggered square pin fins. Energy Convers Manage 2003;44:1787-1803.
[26] Uzol O, Camci C. Heat transfer, pressure loss and flow field measurements downstream of staggered two-row circular and elliptical pin fin arrays. ASME J Heat Transfer 2005; 127:458-71.
[27] Soodphakdee D, Behnia M, Copeland DW. A comparison of fin geometries for heatsinks in laminar forced convection: Part I- round, elliptical, and plate fins in staggered and in-line configurations. Int J Microcircuits and Electronic Packaging 2001;24:68-76.
[28] Moores KA, Joshi YK. Effect of tip clearance on the thermal and hydrodynamic performance of a shrouded pin fin array. ASME J Heat Transfer 2003;125:999-1006.
[29] Wang CY, Cheng P. Multiphase flow and heat transfer in porous media. Adv Heat Transfer 1997;30:183-96.
[30] Nield DA, Bejan A. Convection in porous media. 2nd ed. New York: Springer; 1998.
[31] Mench MM. Fuel cell engines. New Jersey: John Wiley & Sons; 2008.
[32] Tanda G. Heat transfer and pressure drop in a rectangular channel with diamond-shaped elements. Int J Heat Mass Transfer 2001;44:3529-41.
[33] Bejan A, Lorente S. Design with constructal theory. New Jersey: John Wiley & Sons; 2008.
[34] He W, Yi JS, Nguyen TV. Two-phase flow model of the cathode of PEM fuel cells using interdigitated flow fields. AIChE J. 2000;46:2053-64.

[35] Nam JH, Karviany M. Effective diffusivity and water-saturation distribution in single-and two-layer PEMFC diffusion medium. Int J Heat Mass Transfer 2003; 46:4595-4611.

[36] Ansys *Fluent® 12.0 Users Guide Documentation*, Ansys Inc., Southpointe, SAS; 2009.

[37] Pantakar SV. Numerical heat transfer and fluid flow. New York: Hemisphere Publishing Corp.;1980.

[38] Snyman JA. Practical mathematical optimization: an introduction to basic optimization theory and classical and new gradient-based algorithm. New York: Springer; 2005.

[39] Snyman JA, Hay AM. The DYNAMIC-Q optimization method: an alternative to SQP?'. Computer and Mathematics with Applications 2002; 44:1589-98.

[40] de Kock DJ. Optimal tundish methodology in a continuous casting process. PhD Thesis, Department of Mechanical and Aeronautical Engineering, University of Pretoria, 2005.

[41] Bello-Ochende T, Meyer JP, Ighalo FU. Combined numerical optimization and constructal theory for the design of micro-channel heat sinks. Numerical Heat Transfer, Application Part A 2010;58:882-99.

[42] Morris RM, Snyman JA, Meyer JP. Jets in crossflow mixing analysis using computational fluid dynamics and mathematical optimization. AIAA J Propul Power 2007;23(3):618-28.

[43] Ighalo FU, Bello-Ochende T, Meyer JP. Mathematical optimization: application to the design of optimal micro-channel heat sinks. Engenharia Termica 2009;8(1):58-64.

[44] Motsamai OS, Snyman JA, Meyer JP. Optimization of gas turbine combustor mixing for improved exit temperature profile. Heat Transfer Eng. 2010;31(5):402-18.

[45] Le Roux WG, Bello-Ochende T, Meyer JP. Operating conditions of an open and direct solar thermal Brayton cycle with optimised cavity receiver and recuperator. Energy 2011;36:6027-36.

[46] Meyer JP. Constructal law in technology, thermofluid and energy systems, and in design education. Phys Life Rev 2011;8(3)247-48.

[47] Le Roux WG, Bello-Ochende T, Meyer JP. Thermodynamic optimization of an integrated design of a small-scale solar thermal Brayton cycle. Int J Energy Res 2011; DOI: 10.1002/ER.1859.

[48] Chanta VS. An experimental study of end wall heat transfer enhancement for flow past staggered non-conducting pin fin arrays. PhD Thesis, Department of Mechanical Engineering, Texas A & M University, USA; 2003.
[49] Lyall ME. Heat transfer from low aspect ratio pin fins. PhD Thesis, Department of Mechanical Engineering, Virginia Polytechnic Institute and State University, USA; 2006.
[50] Li J., Peterson GP. Geometric optimization of a micro heat sink with liquid flow. IEEE Trans Comp Packag Technol 2006;29(1)145-54.
[51] Husain A, Kim K. Shape optimization of micro-channel heat sink for micro-electronic cooling. IEEE Trans Comp Packag Technol 2008;31(2)322-30.
[52] Fluent Inc., Gambit Version 6 Manuals, 2001.
[53] The Mathworks Inc., MATLAB & Simulink release notes for R2008a, 2008.
[54] L. Tagliafico, G. Tanda, ASME J. Heat Transfer 118 (1996) 805-809.

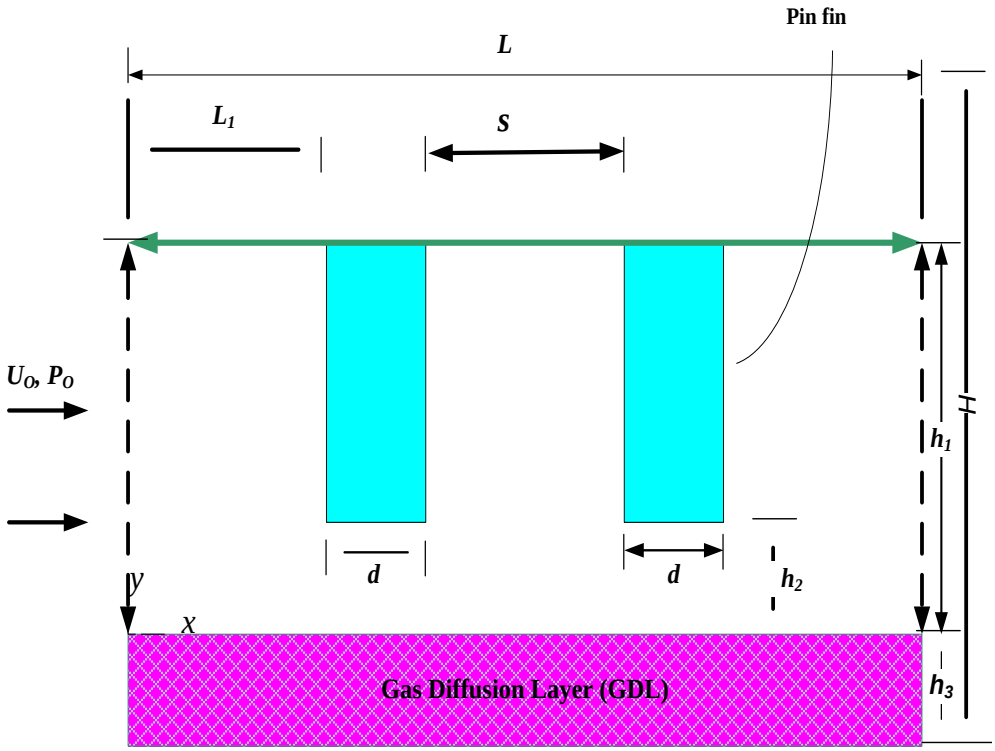

Fig. 1. PEMFC half-cell model with two transverse pin fins along the flow channel.

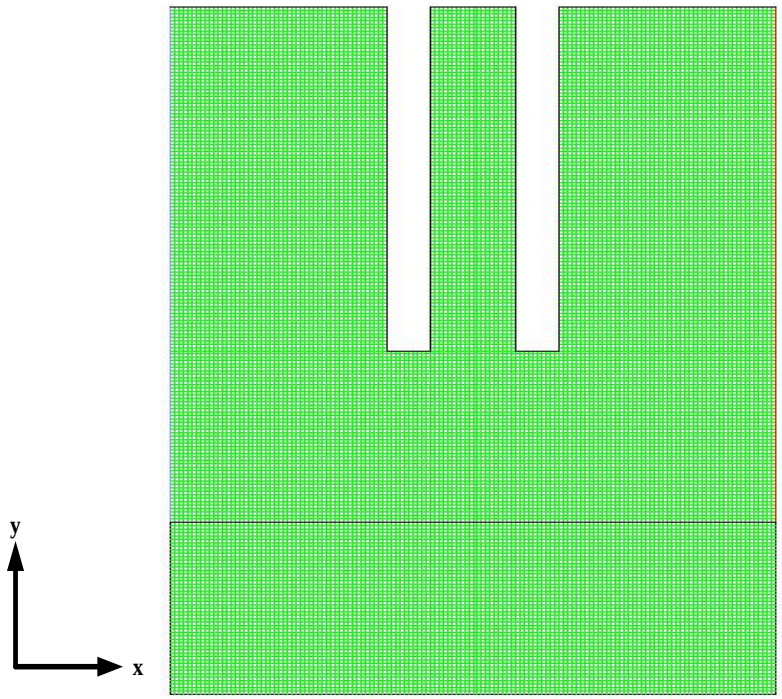

Fig. 2. The representative grid system and computational domain.

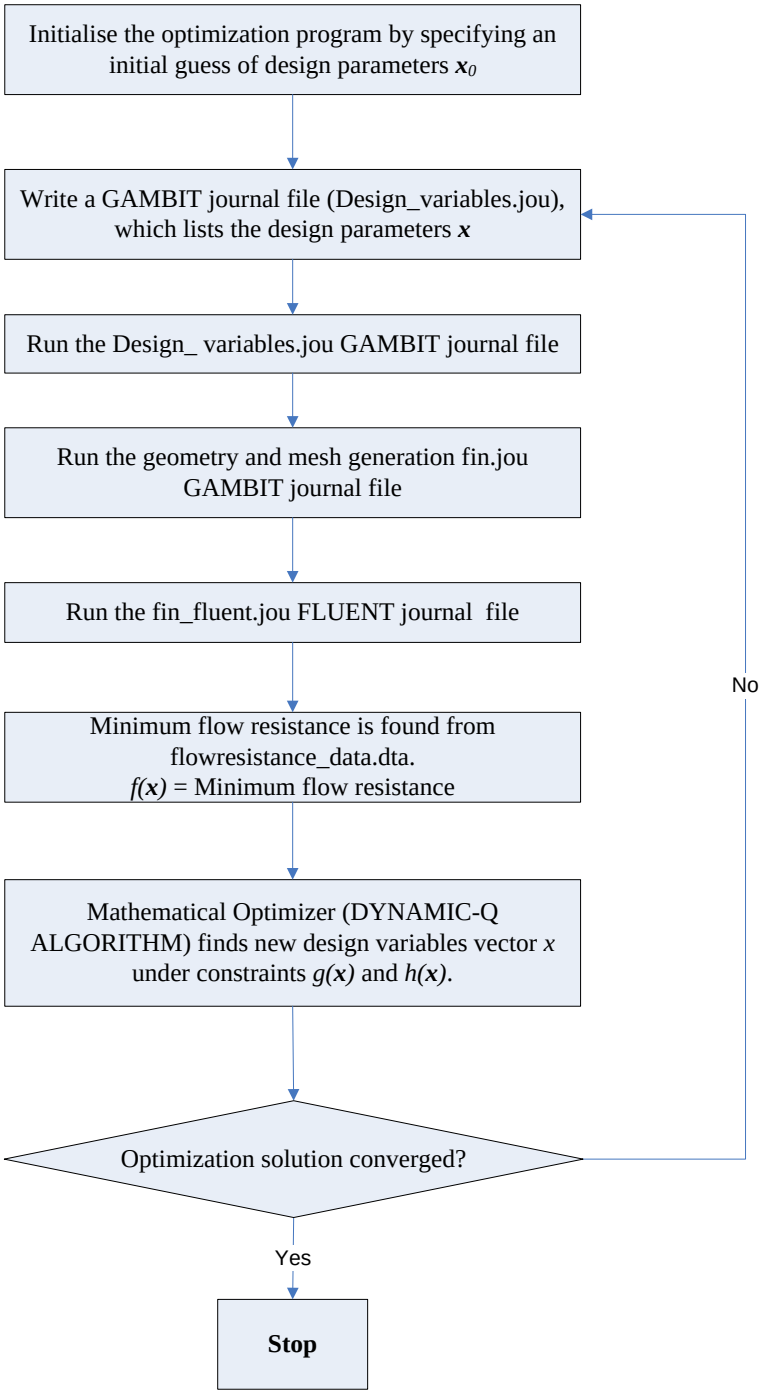

Fig. 3. Optimization automation flow diagram.

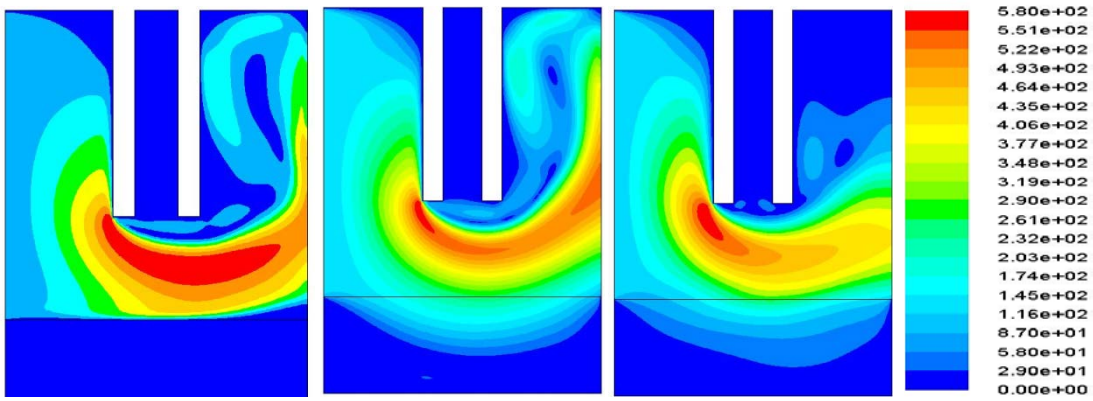

(a) **(b)** **(c)**

Fig. 4. Effect of Reynolds number on the flow field for different flow field configurations ($s/d = 5, \lambda = 0.2$): (a) Re = 50, (b) Re = 150, (c) Re = 250.

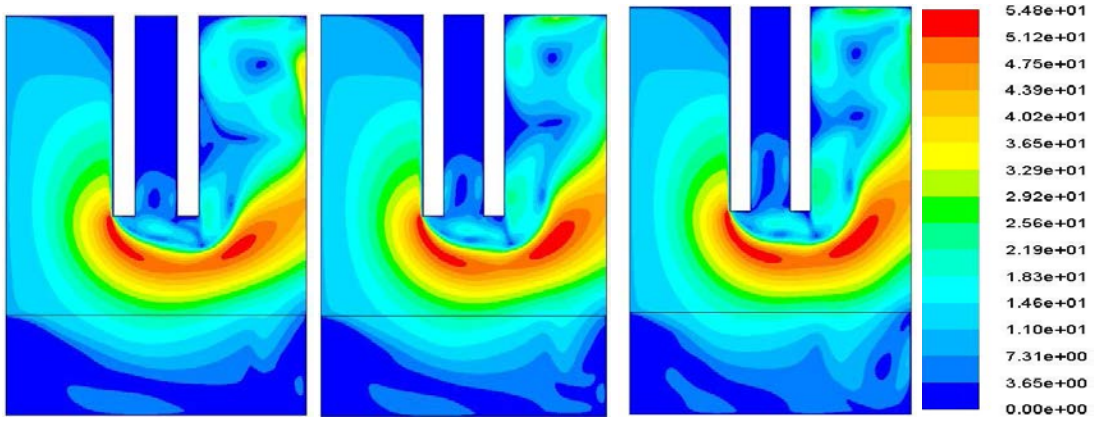

(a) **(b)** **(c)**

Fig. 5. Effect of Reynolds number on the flow field for different flow field configurations (s/d = 5, $\lambda = 0.6$): (a) Re = 50, (b) Re = 150, (c) Re = 250.

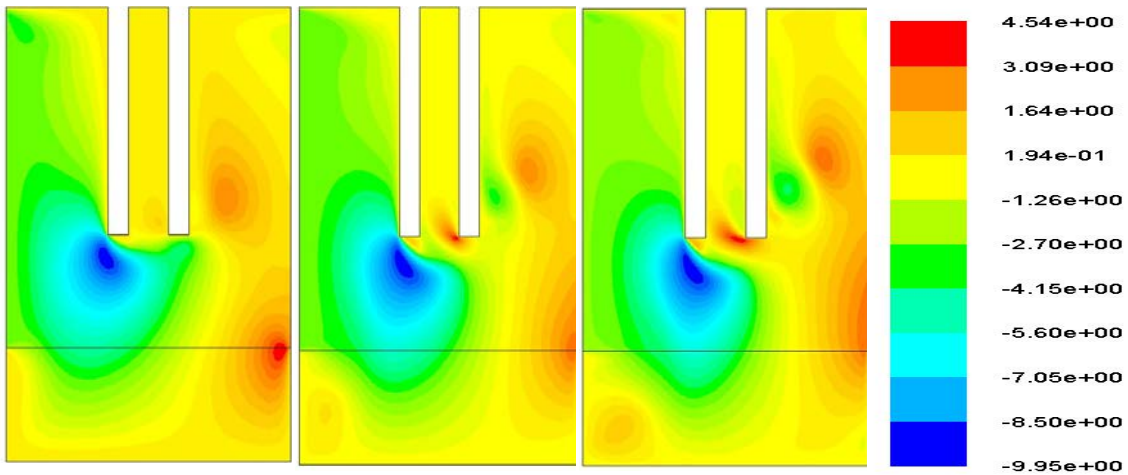

(a) (b) (c)

Fig. 6. Contours of tangential velocity for different flow field configurations (*s/d* = 5, $\lambda = 0.6$): (a) Re = 50, (b) Re = 150, (c) Re = 250.

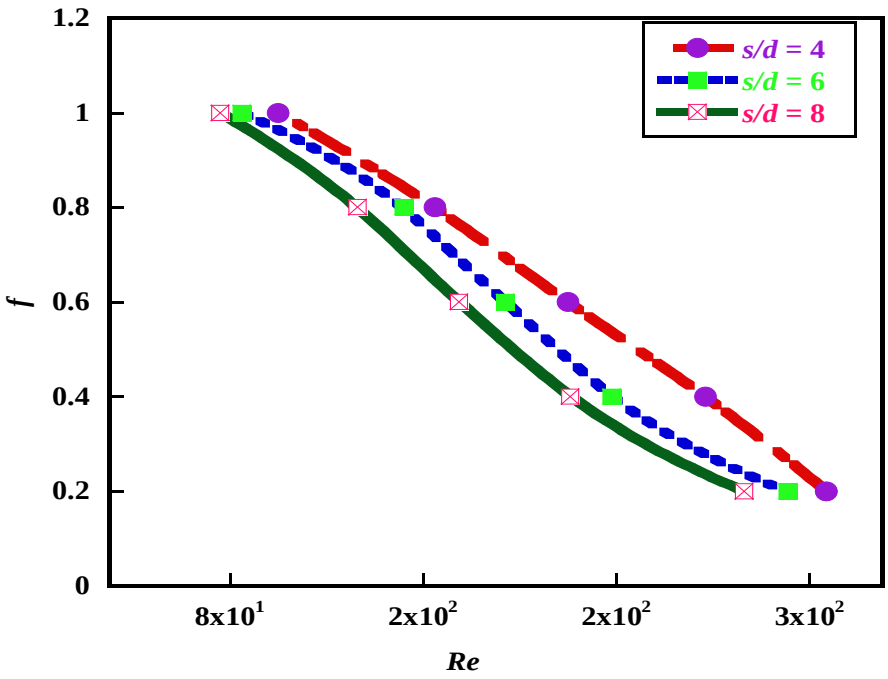

Fig. 7. Cathode gas channel friction factor as a function of the Reynolds number and pitch at a clearance ratio, $\lambda = 0.3$.

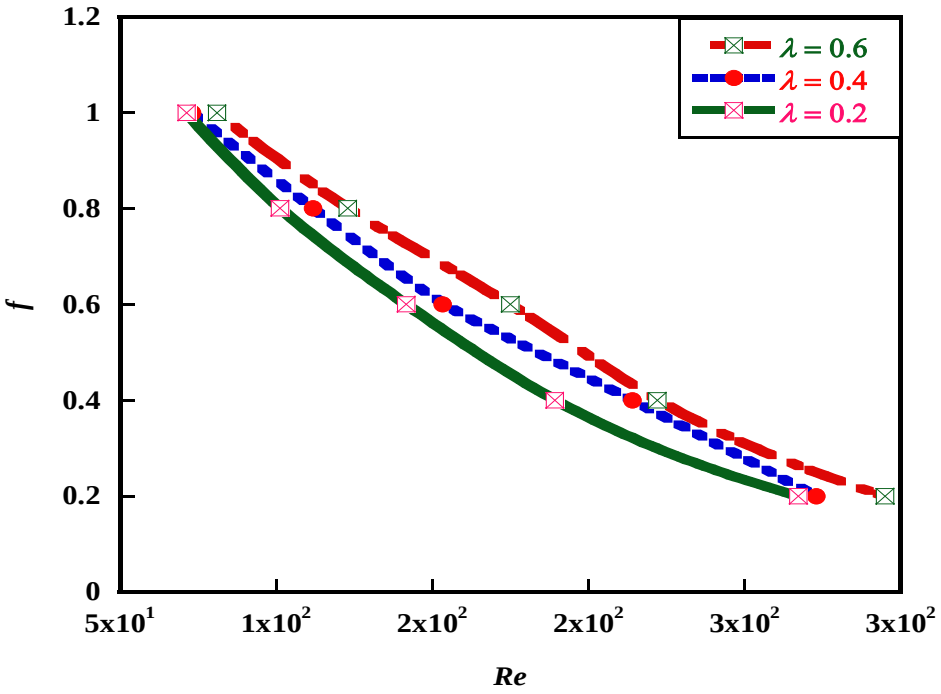

Fig. 8. Cathode gas channel friction factor as a function of the Reynolds number and clearance ratio at a pitch, *s*/*d* = 5.

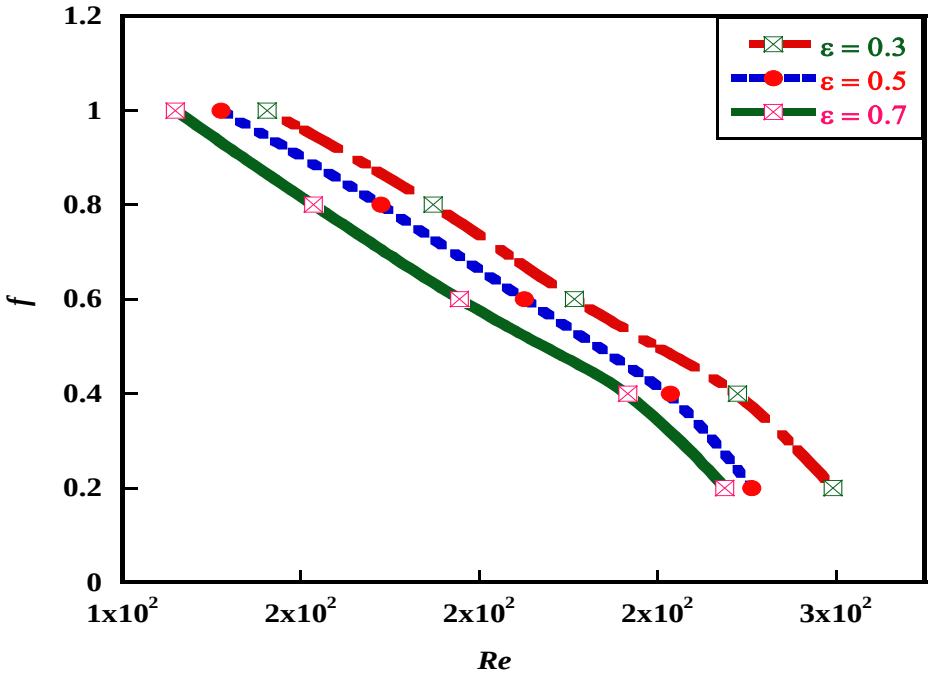

Fig. 9. Cathode gas channel friction factor as a function of the Reynolds number and GDL porosity at a pitch, s/d = 5, and a clearance ratio, λ = 0.3.

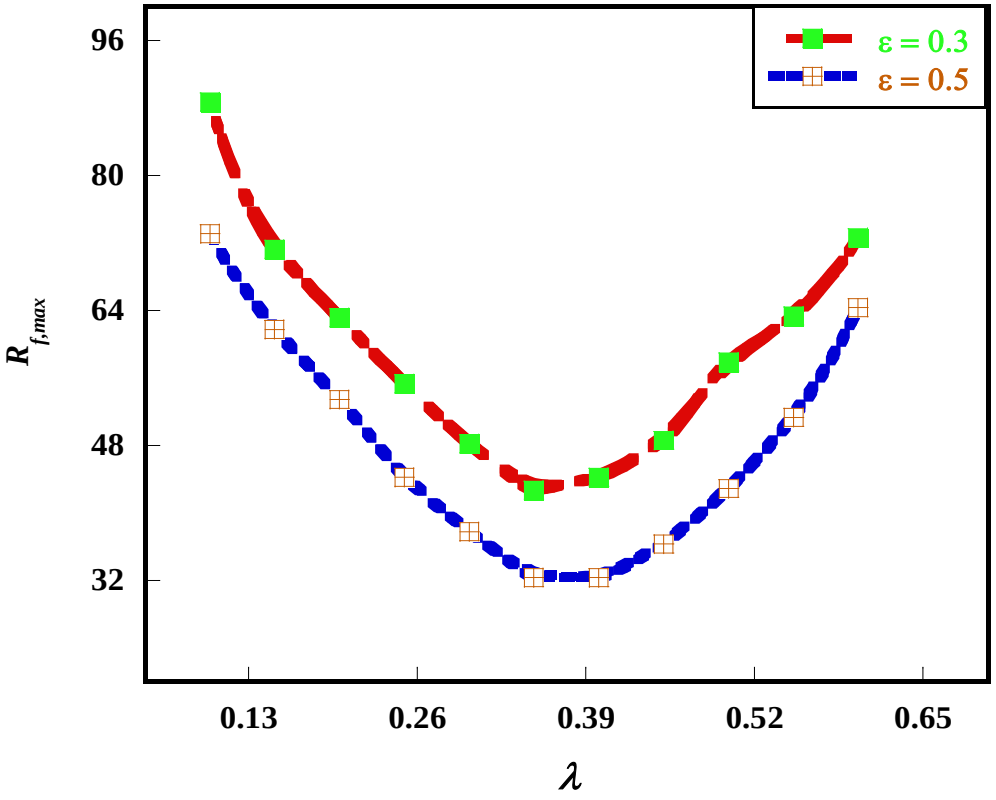

Fig. 10. Effect of optimised clearance ratio on the peak cathode gas channel flow resistance.

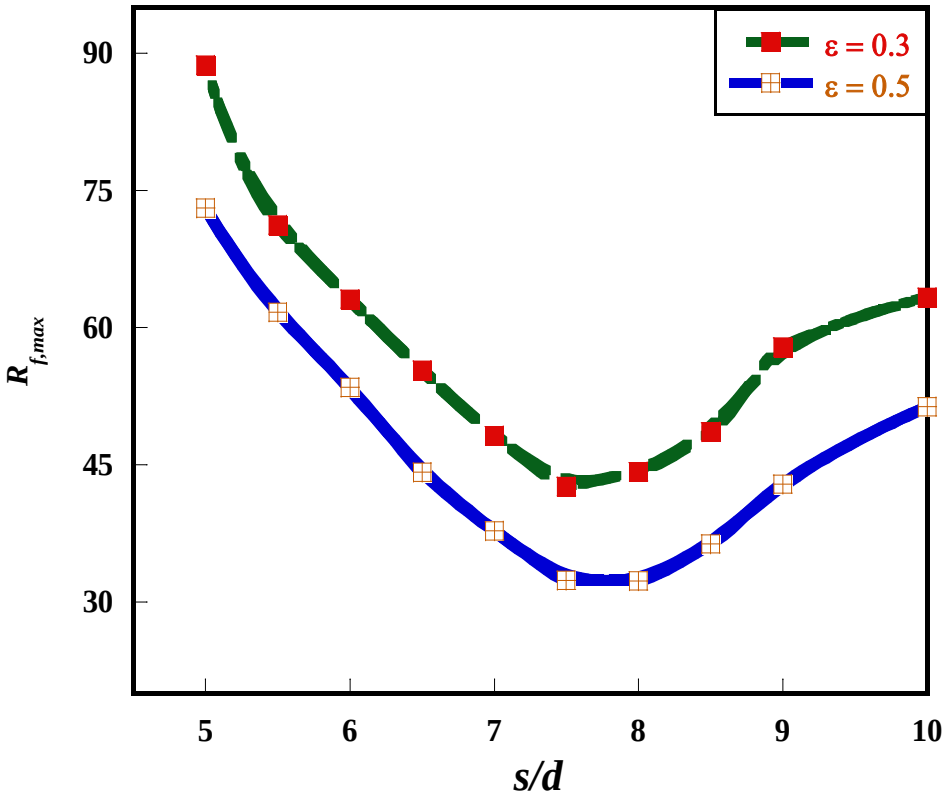

Fig. 11. Effect of optimised pitch on the peak cathode gas channel flow resistance.

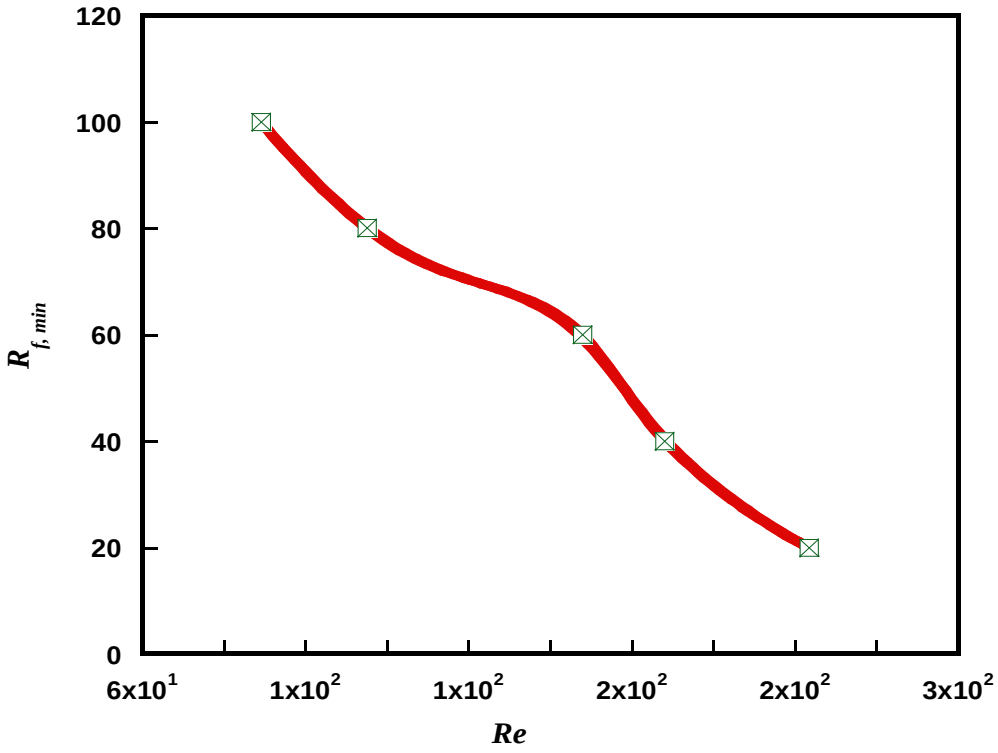

Fig. 12. The minimised cathode gas channel flow resistance as a function of Reynolds number for a fixed GDL porosity, $\varepsilon = 0.5$, and a tip clearance ratio, $\lambda = 0.3$.

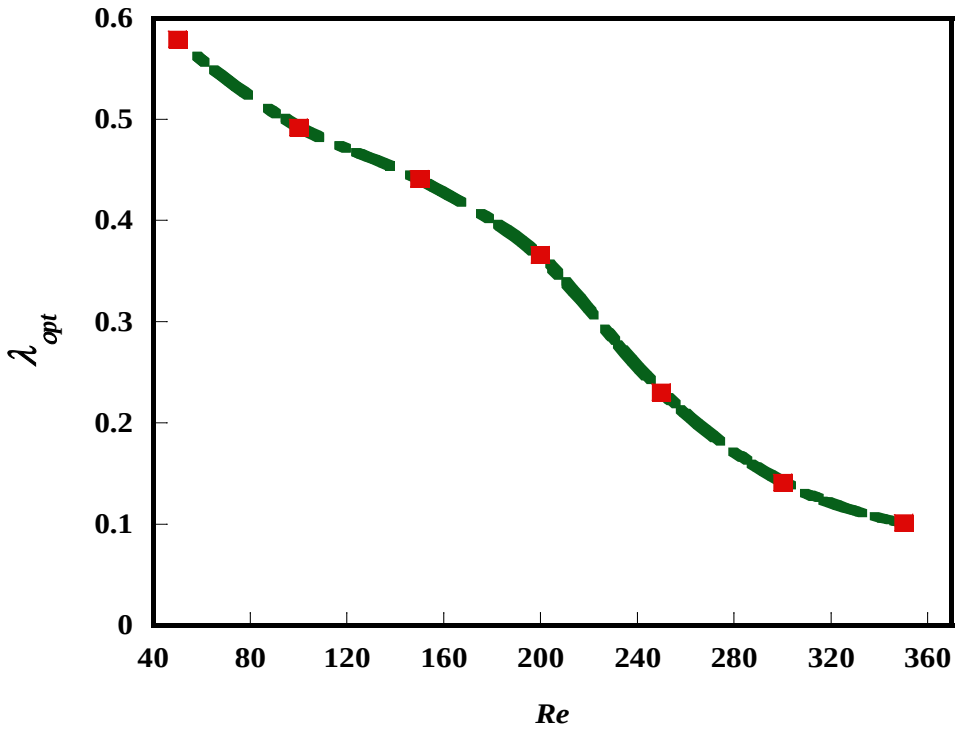

Fig. 13. Optimal clearance ratio as a function of Reynolds number at a fixed pitch, s/d = 5, and a GDL porosity, ε = 0.5.

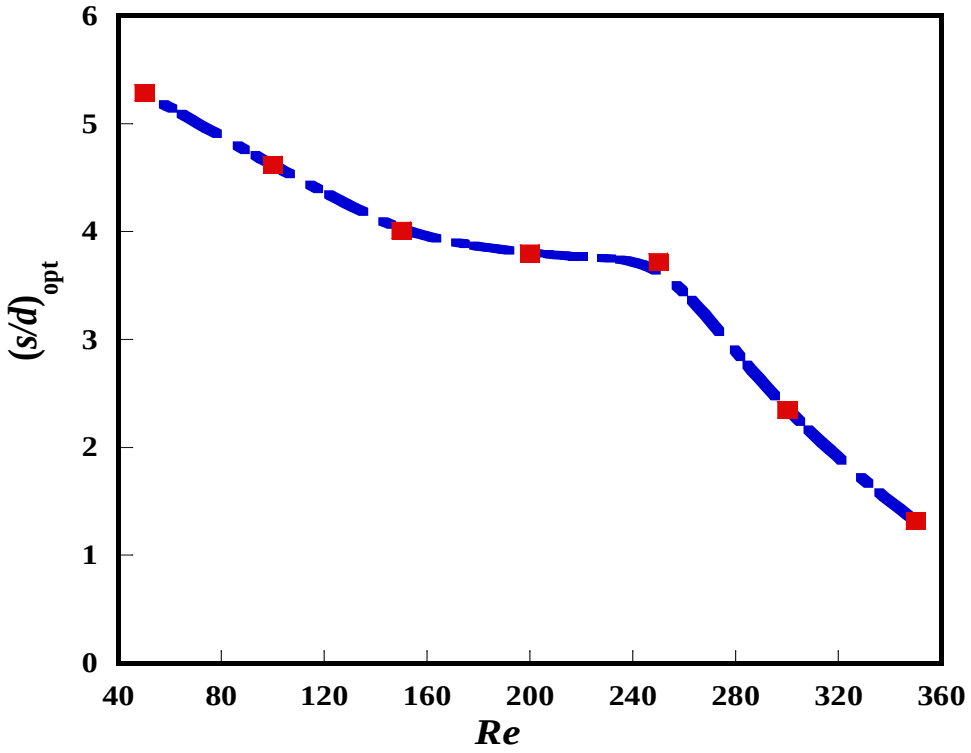

Fig. 14 Optimal pitch as a function of Reynolds number at a fixed clearance ratio, $\lambda = 0.3$, and a GDL porosity, $\varepsilon = 0.5$.

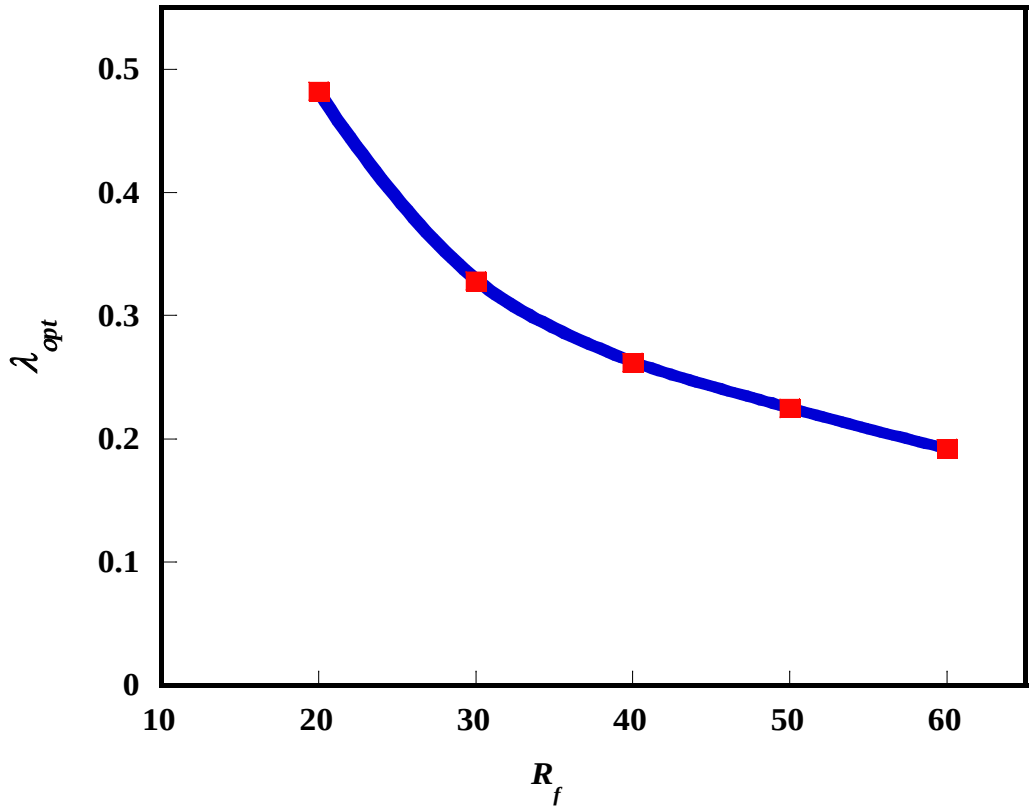

Fig. 15. Effect of channel flow resistance on the optimised clearance ratio at a fixed pitch, *s/d* = 5, and a GDL porosity, ε = 0.5, at Reynolds number of 250.

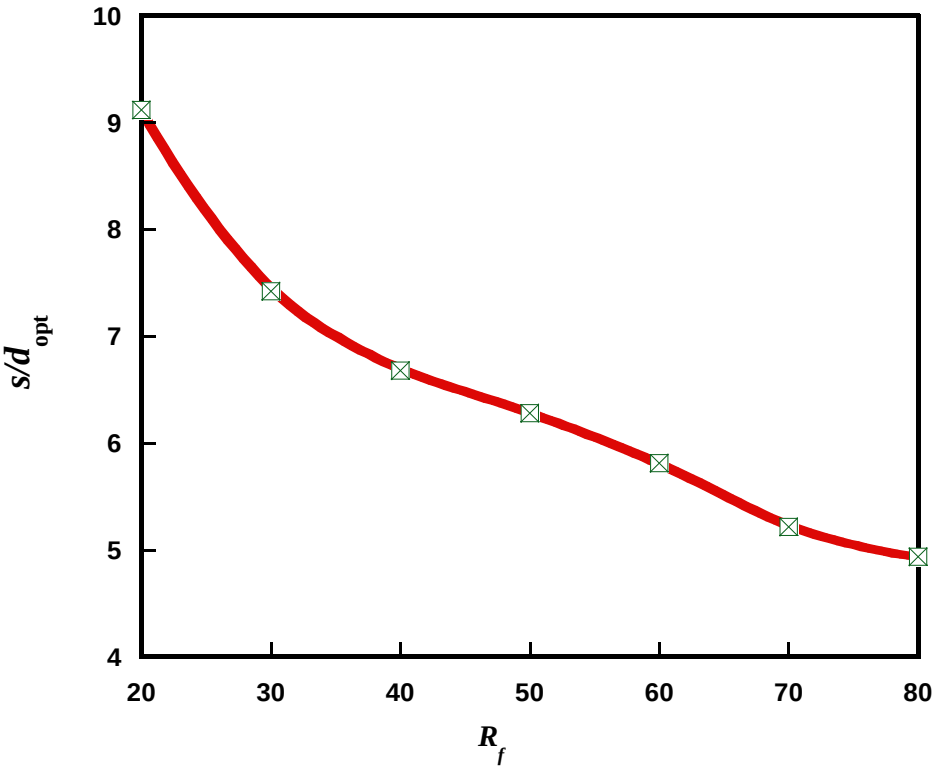

Fig. 16. Effect of channel flow resistance on the optimised pitch at a fixed clearance ratio, $\lambda = 0.3$, and a GDL porosity, $\varepsilon = 0.5$, at a Reynolds number of 250.

.

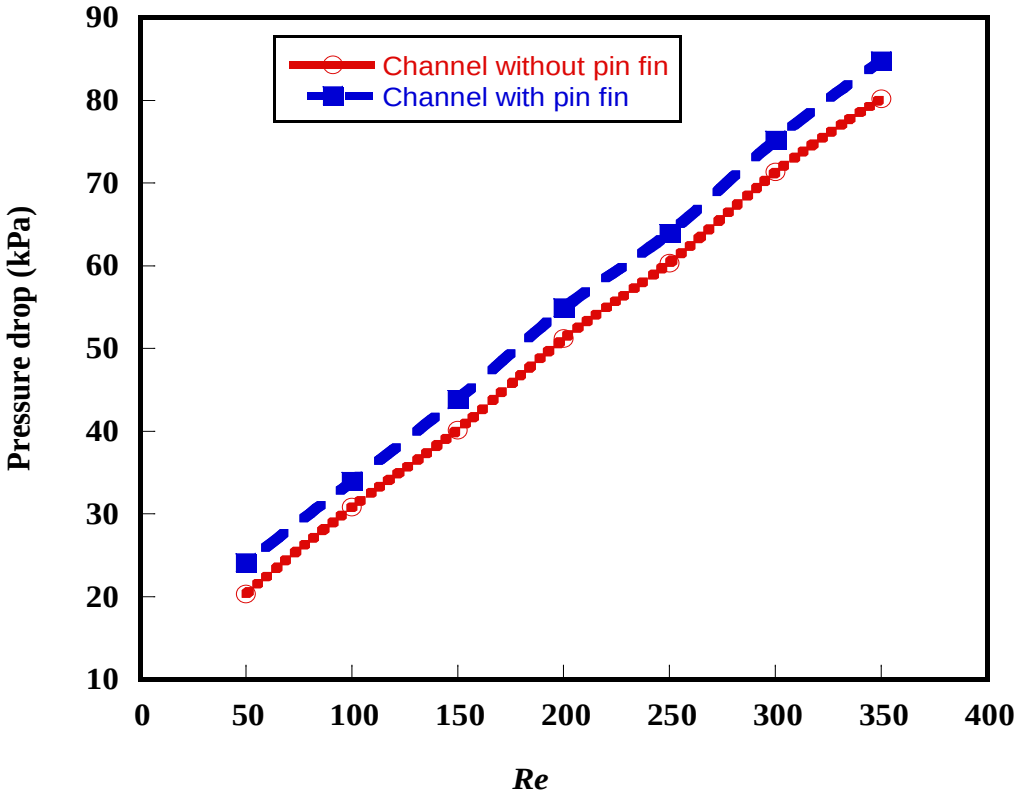

Fig. 17. Cathode gas channel pressure drop as a function of the applied pressure drop for a channel with pin fin ($s/d = 5, \lambda = 0.3$) and one without pin fin.

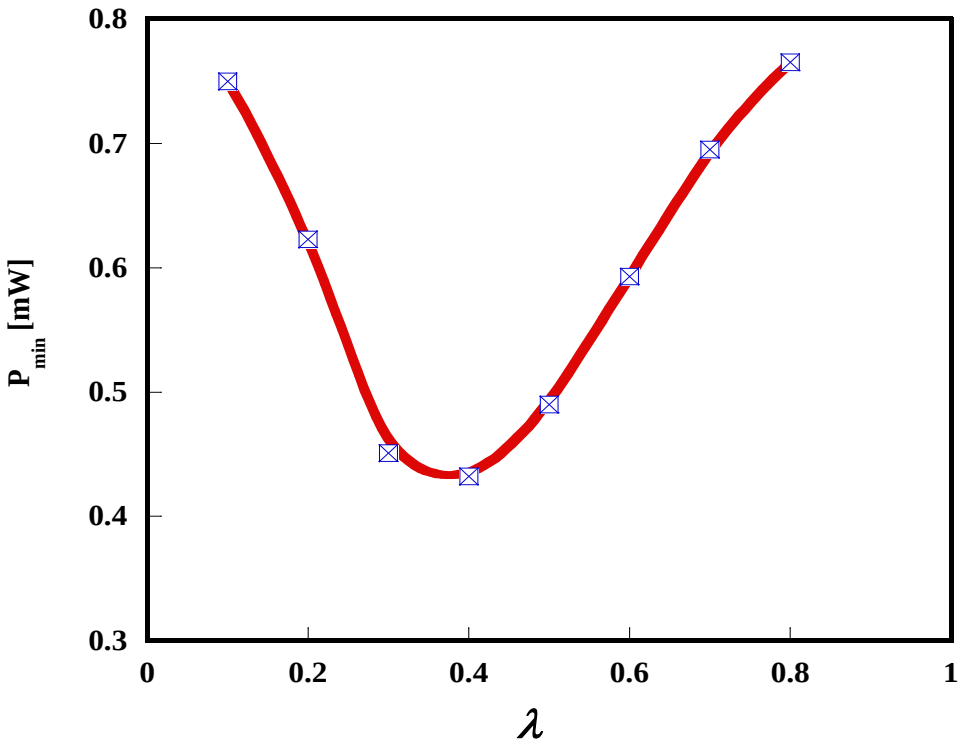

Fig. 18. Pumping power as a function of tip clearance ratio at a pitch, *s/d* = 5, and GDL porosity, ε = 0.6, at a Reynolds number of 250.

Table 1 Parameters of the modeled fuel cell

Channel length (mm)	120
Channel width (mm)	1.0
Channel depth (mm)	1.2
Membrane thickness (mm)	0.036
GDL thickness (mm)	0.21
Membrane porosity	0.5
Cell operating temperature (^{o}C)	70
Cell operating pressure (atm)	3
GDL permeability (m^2)	1.76×10^{-11}
Electric conductivity of GDL $(\Omega^{-1}m^{-1})$	300
Relative humidity	100%